Validation of constitutive model for NiTi alloy based on Experimental Results

M. Branco, & L. Guerreiro
DECivil – Instituto Superior Técnico

J.M. Kelly
University of California at Berkeley

SUMMARY:
The NiTi alloy belongs to the shape memory alloys class of materials, therefore it presents both shape memory effect, for thermally-induced cycling, and superelasticity, for stress-induced cycles. The superelastic property has been the basis of some devices designed to mitigate the earthquake hazard level in structures. Throughout this paper the implementation of a one-dimensional cyclic behavior algorithm to model the NiTi constitutive relation is presented, supported by the thermomechanical formulation developed by Lagoudas and co-workers. The model accounts for isothermal superelastic behavior, incorporating minor hysteretic transformation loops and a new definition of the transformation hardening function. The validation process consisted on the comparison between the results achieved with this algorithm and experimental tests performed at the Pacific Earthquake Engineering Research Center at the University of California at Berkeley. The model was able to replicate the results from the experimental works.

Keywords: Shape memory alloy, thermomechanical algorithm, superelasticity, seismic strengthening.

1. INTRODUCTION

Shape memory alloys (SMAs) are a class of materials, which possess particular thermo-mechanical, thermo-chemical or thermoelectric properties, which allows for the phase transition between two solid phases. The Nickel-Titanium (NiTi) alloy is one example of such materials and it has specific properties, which justify its usage in civil engineering applications. Amongst other properties, this alloy has the capacity of undergo large strain deformation and recover its original shape, through stress or temperature induced cycles. Energy dissipation is also associated with this hysteretic cyclic behavior.

The shape memory alloys may exist in two different crystal configurations, the austenitic and the martensitic. The austenitic phase is stable at higher temperatures and it is stiffer. The martensitic phase is stable for lower temperatures and it is more deformable. At higher temperatures where there is only the austenitic phase for zero stress loading, stress-induced deformation occurs associated with a phase transformation from austenite to martensite (forward transformation). After unloading, the material regains the original austenitic structure (reverse transformation), dissipating energy through hysteretic loops. This behavior is designated as superelasticity [Lagoudas (2008), Aiken et al (1992), Otsuka and Wayman (1998)]. In Figure 1 the shape memory effect and the superelastic properties are presented in the stress-temperature plan. For constant temperature the superelasticity occurs for stress-induced deformation (vertical arrows), for constant stress the temperature-induced deformation leads to the shape memory effect (horizontal arrows).

In the recent decades, several studies were conducted to test the application of SMA technology to civil engineering structures. Most of the projects developed take advantage of the re-centering capacity and the hysteretic energy dissipation, due to superelasticity, to achieve an improvement in seismic behavior of structures [Song et al (2006), Manside Project (1999)].

Ma and Cho (2008) and Dolce et al (2000) explored the re-centering ability and the hysteretic energy dissipation through the design of SMA dampers. Devices composed by pre-stressed austenitic wires, springs and martensitic wires were tested and validated through shake table tests, with good results. Also with the purpose of controlling the residual displacements after the event of an earthquake, Johnson et al (2008) performed shake table testing combined with numerical models of restrainers to control relative displacements at joints in reinforced concrete bridges. Compared to classical solutions, higher energy dissipation and a reduction of 50% in the maximum openings were achieved.
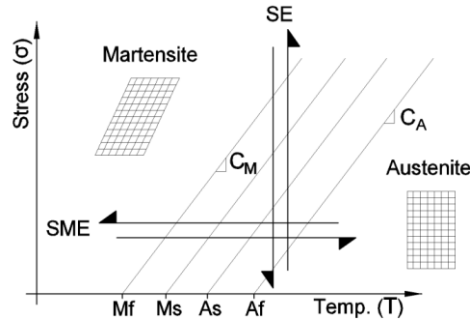

Figure 1. Shape memory effect (SME) and superelasticity (SE) properties presented in the stress-temperature plan. The s and f indexes stand for the start and finish temperatures for the forward (M) and reverse (A) transformations. All temperatures are defined for zero stress conditions.

There are only a few case-studies were the SMA technology was implemented in actual retrofits of existing structures. As examples there is the retrofit of the bell-tower of the Church of S. Giorgio in Trignano Italy [Indirli et al (2001)], the transept tympana of the Basilica of S. Francisco of Assis also in Italy [Croci (2001)] and the rehabilitation of the Sherith Israel Synagogue in San Francisco [Paret and Freeman (2008)]. These few interventions are representative of the improve in performance which is possible to achieve with SMA based devices. Besides all the justifications presented so far, these devices, in series with traditional steel ties, allow a better performance than traditional techniques, due to the control of the applied seismic forces, together with excellent properties against corrosion.

This paper intends to develop an algorithm that models the one-dimensional behavior of NiTi wires, based upon the thermo-mechanical formulation of Lagoudas and co-workers [Lagoudas (2008)]. Its accuracy was tested against experimental results of works performed at the Pacific Earthquake Engineering Research Center in the University of California at Berkeley [Aiken et al (1992)].

2. SUPERELASTIC CONSTITUTIVE MODEL

In the past 25 years, there has been a continuous development of constitutive models that could predict the phase transformation of SMAs. For example, Tanaka (1986) developed an exponential hardening model, which considered the material properties to be kept constant during transformation. Liang and Rogers (1990) used a formulation based upon the Helmotz free energy and a cosine hardening rule for phase transformation. Auricchio and Sacco (1997) used a linear hardening law to model the isothermal superelasticity, by accounting for the change in elastic properties during phase transformation. Further references are addressed in Lagoudas (2008).

The subroutine implemented in this work for the constitutive model of SMA uses the thermo-mechanical framework developed by Boyd and Lagoudas (1996), with some adaptations to account for inner loops and it also uses a more adaptable hardening function. The formulation considers the conservation laws and the basic principles of continuum thermodynamics. Although the original formulation was intended for a three-dimensional body, the algorithm presented in this work uses the one-dimensional simplification [Machado (2007)], accounting only for the axial stress and strain, since only SMA wires were considered in this study. As well, only the superelastic behavior was considered.

For the definition of the constitutive equations, state variables were necessary to evaluate the consistency of the system for each step of the load case. In this formulation, the Gibbs free energy is used as the thermodynamic potential, since for the characterization of SMA is usual to work in the stress-temperature space.

2.1. State variables

At each stress point, an austenitic, a twinned martensite and a detwinned martinsite fraction are possible to coexist. To evaluate the amount of each phase, two internal state variables were considered, the martensitic volume fraction, ξ, and the transformation strain, εt. The variable ξ varies between 0, when the material is in the fully austenitic phase and 1, for the fully martensitic phase. During the transformation phase, ξ assumes values between 0 and 1. In this formulation there is no distinction between twinned phases of the martensite.
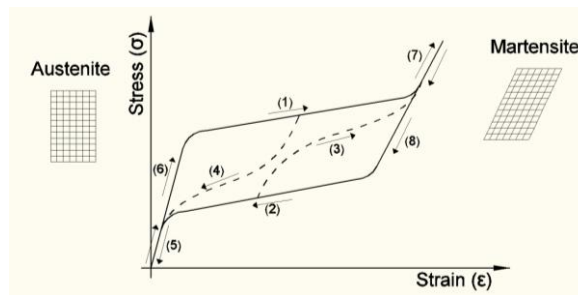

Figure 2. Different load paths for the stress-induced cycles. (1) Major loop loading; (2) Major loop unloading; (3) Minor loop loading; (4) Minor loop unloading; (5-6) austenite elastic behavior; (7-8) martensite elastic behavior

The total strain is the sum of the thermoelastic part and the inelastic strain. The inelastic strain accounts for the transformation strain and the strain associated to plasticity due to yielding. In the formulation adopted, the strain associated to yielding, which is responsible for the residual strain, was assumed to be negligible after a preliminary training stage.

Furthermore, the transformation strain is considered to allow for total recoverable transformation, until transformation strains in the order of 6%. For these range of strains, the use of small strain formulation is acceptable, so the equilibrium equations may be defined in the undeformed configuration. The transformation strains vary from 0, for the austenitic phase, to a maximum transformation strain (H_{Max}), for the full martensitic phase.

As this model does not consider the reorientation of the martensitic variants, the variation of the strain transformation ($\dot{\varepsilon}^t$) is considered equal to the variation of the martensitic fraction ($\dot{\xi}$), times the maximum transformation strain (H_{Max}), which is designated as the flow rule. Therefore, the transformation strain is no longer an independent state variable and for the one-dimensional model, there is a linear relation between ξ and ε^t.

In addition to the previous variables, there were several auxiliary variables considered, so the algorithm could determine which loading path to take, according to its state at the beginning of the step. As shown in Figure 2, there are 8 possible states for the SMA to present at each load step, according to: a) direction of the transformation (forward or reverse); b) type of loop (major/outer or minor/inner); c) reversal in direction; or d) if the material is in the elastic region (austenitic or martensitic) or in the transformation region.

2.2. Outer/major hysteresis loop

If the material is undergoing transformation between austenite and martensite through the outer hysteretic loop, the computation for this case is defined as follow, using the formulation presented by Lagoudas (2008), Boyd and Lagoudas (1996) and Machado (2007).

To define the thermomechanical constitutive relations in the transformation region, the thermodynamic potential given by the Gibbs free energy (G) was considered, which is dependent on the stress (σ), temperature (T), the martensitic volume fraction (ξ) and the transformation strain (ε^t). G was adapted for SMAs in Eq. 2.1.

$$G(\sigma, T, \xi, \varepsilon^t) = -\frac{1}{2\rho}S\sigma^2 - \frac{1}{\rho}\sigma[\alpha(T - T_0) + \varepsilon^t] + c\left[(T - T_0) - T.ln\left(\frac{T}{T_0}\right)\right] - s_0.T + u_0 + \frac{1}{\rho}f(\xi)$$

(2.1)

S is the inverse of the modulus of elasticity (E), α is the thermal expansion coefficient, c is the effective specific heat, s_0 is the effective specific entropy, ρ is the specific mass and u_0 is the effective specific internal energy. As suggested by Lagoudas (2008), all these material constants are linear functions of the state variable ξ. For the approach presented, which does not account for micromechanics, this assumption is acceptable. T0 is the temperature considered as reference and ρ is the specific mass of the material. The function f(ξ) is a transformation hardening function, which will be analyzed ahead.

The inequality of Clausius-Planck (Eq. 2.2) applied to SMAs was obtained from the development of the second law of thermodynamics and applying to the Gibbs free energy (Eq. 2.1). As a result a general thermodynamic force (π) is defined (Eq. 2.3).

$$\left(\sigma.H^{máx} - \rho\frac{\partial G}{\partial \xi}\right)\dot{\xi} = \pi\dot{\xi} \geq 0$$

(2.2)

$$\pi(\sigma, T, \xi) = |\sigma|.H^{máx} + \frac{1}{2}\sigma^2\Delta S + \sigma.\Delta\alpha.(T - T_0) + \rho.\Delta c\left[(T - T_0) - T.ln\left(\frac{T}{T_0}\right)\right] +$$

$$+\rho.\Delta s_0.T - \rho.\Delta u_0 - \frac{\partial f}{\partial \xi}$$

(2.3)

At each instant there are three possible scenarios: a) the forward transformation is in progress; b) the reverse transformation is in progress; c) there is no transformation. When the forward transformation takes place, $\dot{\xi}$ has positive values, as martensite is transformed from austenite. To satisfy the Clausius-Planck inequality (Eq. 2.2), π has to assume positive values. For the reverse transformation, $\dot{\xi}$ assumes negative values, therefore π also has to present negative values. In the third case where there is no transformation ($\dot{\xi}$=0), π may assume any value.

These considerations may be rewritten in the form of a transformation function (Φ) (Eq.2.4), which represents the transformation surface between ξ=0 and ξ=1, and for each transformation path, Φ satisfies the Clausius-Planck relation. The phase transformation is assumed to begin when the thermodinamical force (π) reaches a critical value Y, constant for the entire transformation phase. Therefore, according to Eq. 2.4, when either the forward (Φ^+) or the reverse (Φ^-) transformations are undergone, Φ equals zero. Furthermore Eq. 2.4 may be rewritten in the equivalent format of the Kuhn-Tucker condition, as $\Phi\dot{\xi} = 0$.

$$\begin{cases} \Phi^+(\sigma, T, \xi) = \pi - Y \leq 0, \text{ for } \dot{\xi} \geq 0 \text{ (forward)} \\ \Phi^-(\sigma, T, \xi) = -\pi - Y \leq 0, \text{ for } \dot{\xi} \leq 0 \text{ (reverse)} \end{cases}$$

(2.4)

In addition, the phase transformation has to be kept on the transformation surface, by satisfying the consistency condition of $\dot{\Phi}=0$. This condition assumes that the SMA has a rate-independent behavior due to its diffusionless nature, whereas the loading/unloading process is rapid enough to avoid any diffusion-controlled process. This assumption is considered as a valid approximation for the spectrum of frequencies tested in this study, according to experimental results [Lagoudas (2008)].

2.3. Inner/minor hysteresis loops

 The definition of the minor hysteresis loops is necessary when the forward transformation halts before reaching the full martensitic phase (4 in Figure 2) or when the reverse transformation changes direction before recovering its austenite shape (3 in Figure 2). As the objective of this work is to achieve a simple model that could simulate the superelastic behavior of SMA wires, a simpler formulation was considered taking the major hysteresis loop formulation as background. For a more accurate model, Bo and Lagoudas (1999) developed a thermomechanical formulation, which could be incorporated in the major loop model, which used the Preisach model.

A few assumptions were considered: a) the phase transformation will start immediately after the reversal of the loop; b) the amount of energy dissipated during a minor loop phase transformation cycles should be variable depending on the martensitic volume fraction at the reversal point (ξ_r^n) of the nth order branch of the hysteresis curve; c) when approaching $\xi=0$ for the reverse transformation or when approaching $\xi=1$ for the forward transformation, the minor loop tends to the configuration of the major loop.

The parameter Y which was assumed as a constant for the outer loop, now it is considered as a variable Y_n depending on ξ (martensitic volume fraction at each step) and ξ_r^n. When a reversal takes place, the transformation functions for forward and reverse transformation have to be both null for the same value of ξ, according to assumption a). Therefore the value of Y_n has to be different from Y_{n-1}, in order for the Kuhn-Tucker condition to be valid.

Y_n was considered to have an exponential distribution, as presented in Eq. 2.5, to behave closer to the experimental results. The forward and reverse transformations where defined separately to satisfy assumption c). Consequently, for the minor loops to tend to the major loops in the vicinity of $\xi=0$ or $\xi=1$, b has to be equal to Y, as defined for the major hysteretic loop.

$$\begin{cases} Y_n^+ = A_n\left(e^{\gamma(1-\xi)} - 1\right) + b \,, for\ \dot{\xi} \geq 0\ (forward) \\ Y_n^- = A_n\left(e^{\gamma\xi} - 1\right) + b, \ \ for\ \dot{\xi} \leq 0\ (reverse) \end{cases}$$

(2.5)

Finally, the variable A_n and the variable γ have to be determined, so this formulation may be fully characterized. While γ is a material parameter, which is determined directly from experimental results, A_n, requires further computation. An is constant for each sub-loop and it has to be determined every time a reversal in the transformation direction occurs, according to Eq. 2.6.

$$A_n = \begin{cases} \dfrac{\pi - Y}{e^{[\gamma(1-\xi_r^n)]} - 1} \,, for\ \dot{\xi} \geq 0\ (forward) \\ \dfrac{-\pi - Y}{e^{(\gamma \cdot \xi_r^n)} - 1} \,, \ for\ \dot{\xi} \leq 0\ (reverse) \end{cases}$$

(2.6)

2.4. Hardening function

The full characterization of this constitutive model is concluded with the definition of the hardening

function f(ξ). This function is used to account for the interactions between the two phases in the transformation region. The function adopted is presented in Eq. 2.7. The parameters defined for this model were considered the same as for the smooth hardening model developed by Machado (2007).

$$\frac{\partial f}{\partial \xi} = \begin{cases} a_1\left[n_2\left(1 - e^{-n_1\xi}\right) + n_4\left(e^{n_3\xi} - 1\right)\right], for\ \dot{\xi} \geq 0\ (forward) \\ a_2\left[n_6\left(1 - e^{-n_5\xi}\right) + n_8\left(e^{n_7\xi} - 1\right)\right],\ for\ \dot{\xi} \leq 0\ (reverse) \end{cases}$$

(2.7)

2.5. Return mapping algorithm

For each time step, this model receives the total strain and delivers the updated value for stress (σ) and for the martensitic volume fraction (ξ) at the end of the step. Therefore, the solution is achieved by solving a non-linear system of two unknowns and two equations, which are the transformation function and the strain equation. To overcome this situation, an iterative procedure was implemented.

The subroutine uses a return mapping algorithm as defined to determine the value of the state variable ξ and the stress value at the end of each step. In this case, the convex cutting plane algorithm was used. This method is suitable for numerical integration of rate independent inelastic constitutive models, as the present one. By using a predictor-corrector formulation, first a thermoelastic step is tested and case it does not respect the consistency condition, a correction is applied. The formulation used is only valid for isothermal loading, as only the superelastic behavior is being modeled in this work. In Machado (2007) this formulation is expanded to account for thermal variation.

For each time step, the transformation function (Φ) and the stress are computed for a new level of total strain, assuming there is no change in the martensitic volume fraction. As previously referred the Kuhn-Tucker condition imposes that if an increase in strain occurs in the transformation region, then an increase in the martensitic volume fraction also has to happen, so the transformation function may be equal to zero. If the Kuhn-Tucker condition is not observed within a tolerance of δ<10-8, there is the need to correct ξ according to the following equations (Eq. 2.8). This iterative procedure will carry on until the transformation function equals zero.

$$\Delta\xi_{n+1}^{(k)} = \frac{\Phi_{n+1}^{(k)}}{\pm\left(\frac{\partial\Phi_{n+1}^{(k)}}{\partial\sigma}\right)^2 . E - \frac{\partial\Phi_{n+1}^{(k)}}{\partial\xi}}$$

(2.8)

3. VALIDATION

For the purpose of this work, a finite element program was developed in MatLab ®, which could account for physical non-linear behavior at the section level. In addition to static analysis, the program was developed to compute modal analysis and time history dynamic analysis using the Newmark method and to incorporate the previous constitutive model, which simulates the SMAs superelastic cyclic behavior. The model performs two-dimensional analysis, where frame elements connected through nodes are used to model the structure under study. The section geometry of each element and the material constants necessary for the definition of the constitutive models are defined prior to the run of the program.

3.1. Experimental tests

After the presentation of the thermomechanical model used to simulate the superelastic behavior of NiTi wires, a validation based on experimental results was conducted. The model performance was

matched up to the results of quasi-static cyclic tensile tests and shake table tests performed by Aiken, Nims and Kelly (1992) at the Pacific Earthquake Engineering Research Center of the University of California at Berkeley.

The shake table measures 1.42 m by 1.22 m in plan, with one horizontal degree-of-freedom and a payload capacity of 45 kN. The tested model was a three story high moment-resistant steel frame. The specimen has 0.91 m x 1.22 m in plan and a total height of 1.83 m. A total weight of 18.9kN was equally distributed for each floor. The bare model presented damping of 0.5% and its three translational frequencies in the direction of excitation were 2.6 Hz, 10.9 Hz and 24.5 Hz.

In these tests, NiTi wires were used as part of the cross-bracing system at each level, placed at each diagonal in series with a steel bar for a 0.1m length. This configuration allowed the wires to be kept always in tension. A 3% pre-strain was applied to the wires in order for them to work in the transformation region and therefore to increase the hysteretic energy dissipation. The specimen was tested under a normalized version of the Zacatula ground motion, which was scaled to consider a peak ground motion of 0.1 g (0.98 m/s2).

The steel structure was considered to have an elastic behavior throughout the tests, assuming that yielding of the steel does not occur. Furthermore, a 2-d model was implemented. The modal frequencies, the accelerations and displacements at each level were matched between the bare specimen and the numerical model, by changing the bending stiffness of the vertical elements. The results obtained are very similar between the experiment and numerical model.

Table 3.1. Material parameters determined according to typical values considered for the calibration of the numerical model.

α^A [K^{-1}]	α^M [K^{-1}]	Δc [J.kg^{-1}.K^{-1}.]	C^A [kPa/K]	C^M [kPa/K]	ρ [kg/m^3]
22.0x10^{-6}	22.0x10^{-6}	0.0	7000	7000	6500

Table 3.2. Material parameters determined from the experimental results for the calibration of the model.

Material Parameters	Static	Dynamic	Material Parameters	Static	Dynamic
E^A [kPa]	24.0x10^6	70.0x10^6	T_0 [K]	295	295
E^M [kPa]	20.0x10^6	60.0x10^6	γ	50	30
σ_{MS} [kPa]	390x10^3	400x10^3	$n1=n5$	20	15
σ_{MF} [kPa]	700x10^3	950x10^3	$n2=n6$	0.6	1.8
σ_{AS} [kPa]	450x10^3	700x10^3	$n3=n7$	4.4	1.5
σ_{AF} [kPa]	250x10^3	200x10^3	$n4=n8$	0.02	1.2
H^{Max} [%]	5.2	2.7			

3.2. Material parameters

Several material parameters were characterized for the implementation of this constitutive model. The parameters defined in Table 3.1 were determined according to literature [Lagoudas (2008), Aiken et al (1992), Machado (2007)], where CM and CA are the zero stress slops of transformation regions into martensite and austenite. Additionally, the young modulus (E), the stress values for the start and end of the forward (M) and reverse transformations (A), the maximum uniaxial transformation strain

(H_{Max}) and the working temperature (T_0) where determined from the experimental tensile results. Also the parameters γ for the inner loops and n# for the hardening function were determined iteratively. All the values obtained are gathered in Table 3.2 for the tests in static and dynamic conditions.

3.3. Results

At a first stage, the algorithm was tested against three quasi-static cyclic tensile tests. After these preliminary tests, the three-story structure was tested for the Zacatula ground motion. In the first test the wires were tested with strains up to 5%. In the second test the maximum strain was increased to 8%. For the third test, the wires were subjected to a pre-stress of 3% strain and cycled in a 4% strain interval in dynamic conditions. The results for the three tests are overlapped below for the numerical model and the experimental results, in Figure 3 and Figure 4.

In the first two cyclic tensile tests (Figure 3), the experimental results present residual deformation due to plastic strain associated with crystal slippage, for the reverse transformation. Discrepancies up to 1% residual strain were observed, since this phenomenon was not considered in this formulation. Nevertheless, the model was capable to predict the forward transformation outer loop and the reverse transformation inner loops, especially for higher strains.
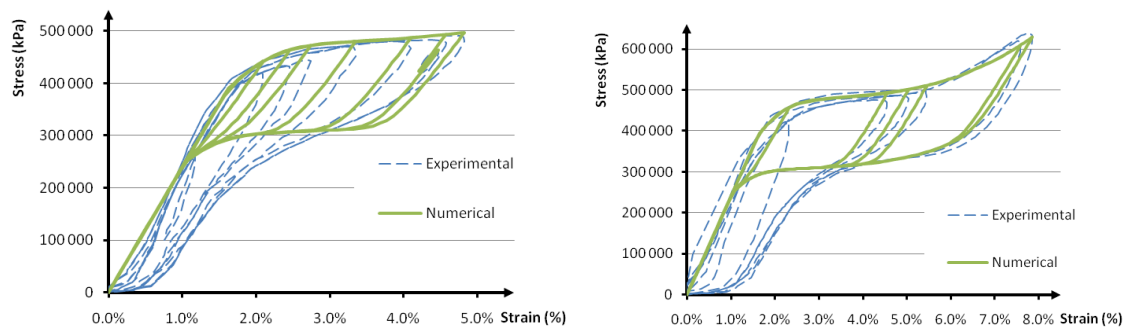

Figure 3. Comparison between experimental data and numerical model for small strain (left) and large strain (right) tensile test.
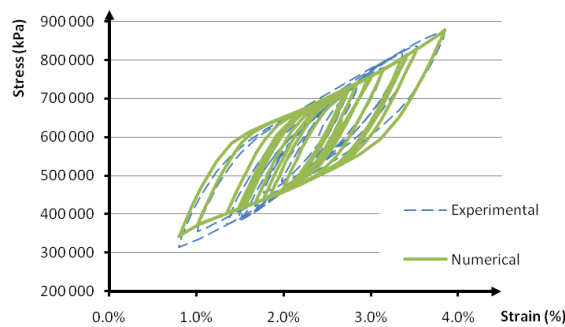

Figure 4. Comparison between experimental data and numerical model for 3% pre-strain tensile test.

After the model was calibrated for the first two tests, its performance was tested when pre-strain is added in dynamic conditions (Figure 4). In this case, the material worked only in the transformation region, which allowed for an increase in the energy dissipation due to hysteretic behavior. Furthermore, the effect of residual deformation is negligible, as a result the model adapts more accurately to both the forward and reverse transformations.

As the ability for this model to simulate the behavior of NiTi wires was proved for cyclic tensile tests, then it was tested when implemented into a three-story steel structure. In Table 3.3 the comparison between the displacements and accelerations at each level are presented for the numerical model and

for the experimental shake table results. Once again the numerical model results are close to the experimental ones, as differences range up to 17%. In Figure 5 the hysteretic behavior of the NiTi wires placed in the bracing system of the structure is presented, as obtained from the numerical model and compared against the envelope of the experimental results. The envelope has a similar shape to the numerical results, although there is some discrepancy for lower strains. The differences in results could be associated to the use of a planar model to simulate a 3-dimensional structure, to some inelastic behavior from the steel elements, to an inaccurate estimate of the pre-strain in every diagonal, besides issues related to changes in the NiTi behavior for dynamic solicitations.

Table 3.3. Comparison between experimental results and numerical model for the specimens tested in the shake table at UC Berkeley.

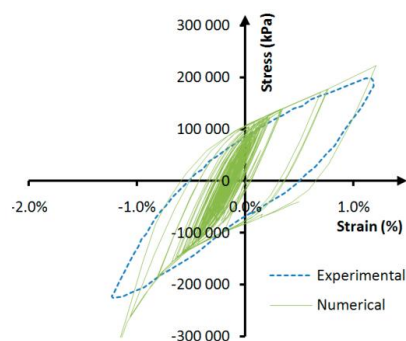| Level	Acceleration (m/s^2)			Displacement (m)		
	Experimental	Numerical	Ratio (Exp/Num)	Experimental	Numerical	Ratio (Exp/Num)
3	3.04	3.67	0.83	5.84x10^{-03}	6.34x10^{-03}	0.92
2	2.58	2.41	1.07	4.20x10^{-03}	4.20x10^{-03}	1.00
1	1.44	1.43	1.00	2.05x10^{-03}	1.82x10^{-03}	1.12

Figure 5. Hysteretic behavior of NiTi wire in numerical model subjected to ground motion compared against the experimental results envelope

4. FINAL REMARKS

This paper addressed the implementation of a superelastic constitutive model for the NiTi alloy in MatLab, which could work as a tool for more elaborate analysis, with the ultimate goal of designing SMA based devices for seismic retrofitting of structures.

The framework developed by Lagoudas and co-workers was used to simulate the superelastic behavior of the NiTi alloy, in isothermal conditions. The Gibbs free energy was considered as the thermodynamic potential, which was developed into a transformation function, which defined the transformation surface for the forward and reverse transformations. This formulation was further adapted to account for the minor hysteretic loops when a reversal occurs during transformation.

The model was validated and tested against experimental results performed at the Pacific Earthquake Research Center at UC Berkeley. Preliminary cyclic tensile testing for NiTi wires with and without pre-strain was used to define the hardening function and the material parameters for the model. The results obtained in the numerical model presented a behavior similar to the experimental results.

Finally the validated model was implemented in a two-dimensional finite element model in order to simulate the behavior of a small-scale steel structure with NiTi wires introduced in the cross-bracing system and subjected to a ground motion in a shake table. The results were also satisfactory, as the performance of the model, in terms of accelerations and displacements were close to the experimental

results. The hysteretic behavior of the NiTi wires stands out the energy dissipation capability this material has and its potential in civil engineering applications also associated with the re-centering ability.

ACKNOWLEDGMENTS

REFERENCES

Lagoudas, D. (2008) Shape Memory Alloys – Modeling and Engineering Applications. Springer, New York.

Aiken, I.; Nims, D.; Kelly, J.M. (1992) Bulletin of the New Zeland National Society for Earthquake Engineering 25 (3) 175-193

Otsuka, K.; Wayman, C.M. (1998) Shape Memory Materials. Cambridge University Press, Cambridge.

Song. G.; Ma, N.; Li, H.N. (2006) Applications of shape memory alloys in civil structures – Engineering Structures, Elsevier, n.28, pp.1266-1274.

Manside Project (1999) Memory Alloys for New Seismic Isolation and Energy Dissipation Devices, Workshop Proceedings. Rome, January 28-29.

Ma, H.; Cho, C (2008) Feasibility study on a supereslastic sma damper with re-centring capability - Materials Science and Engineering A 473, 290–296, Elsevier.

Dolce, M.; Cardone, D.; Marnetto, R. (2000) Implementation and testing of passive control devices based on shape memory alloys - Earthquake Engng Struct. Dyn; 29: 945-968.

Johnson, R.; Padgett, J.E.; Maragakis, M.E. (2008) Large scale testing of nitinol shape memory alloy devices for retrofitting of bridges - Smart Mater. Struct. 17 035018 (10pp).

Indirli, M.; Castellano, M.; Clemente, P.; Martelli, A. (2001) "Demo-application of shape memory alloy devices: The rehabilitation of the S. Giorgio Church bell-tower," Proceedings of SPIE, Smart Structures and Materials.

Croci, G. (2001) "Strenghtening of the Basilica of St. Francis of Assissi after the 1997 Earthquake", Structural Engineering International.

Paret, T.F.; Freeman, S.A. (2008) Using traditional and innovative approaches in the seismic evaluation and strengthening of a historic unreinforced masonry synagogue. – Engineering Structures 30 2114-2126.

Tanaka, K. (1986) A thermomechanical sketch of shape memory effect: One-dimensional tensile behavior, Res. Mechanica 18, 251-263

Liang, C.; Rogers, C.A. (1990) One-dimensional thermomechanical constitutive relations for shape memory materials, Journal of Intelligent Material Systems and Structures 1 (1990) 207-234

Auricchio, F.; Sacco, E. (1997) A one-dimensional model for superelastic shape memory alloys with different elastic properties between austenite and martensite, International Journal of Non-Linear Mechanics 32 (6) 1101-1114

Boyd, J.G.; Lagoudas, D.C. (1996) A thermodynamical constitutive model for shape memory materials, Part I: The monolithic shape memory alloy, International Journal of Plasticity 12 (6) 805-842.

Machado, L. (2007) Shape Memory Alloys for Vibraion Isolation and Damping, Dissertation for the degree of Doctor of Philosophy, Texas A&M University

Bo, Z.; Lagoudas, D. (1999) Thermomechanical modeling of polycrystalline SMAs under cyclic loading, Part IV: modeling of minor hysteresis loops. International Journal of Engineering Science 37 (1999) 1205-1249